Distributed plasticity approach for the nonlinear structural assessment of offshore wind turbine

Article *in* International Journal of Naval Architecture and Ocean Engineering · October 2020

DOI: 10.1016/j.ijnaoe.2020.09.003

4 authors:

Thanh-Tuan Tran
Kunsan National University
26 PUBLICATIONS **67** CITATIONS
SEE PROFILE

Mosaruf Hussan
The University of Queensland
15 PUBLICATIONS **51** CITATIONS
SEE PROFILE

Doo Kie Kim
Kongju National University
155 PUBLICATIONS **990** CITATIONS
SEE PROFILE

Phu-Cuong Nguyen
Ho Chi Minh City Open University
56 PUBLICATIONS **308** CITATIONS
SEE PROFILE

International Journal of Naval Architecture and Ocean Engineering 12 (2020) 743–754

Contents lists available at ScienceDirect

International Journal of Naval Architecture and Ocean Engineering

journal homepage: http://www.journals.elsevier.com/international-journal-of-naval-architecture-and-ocean-engineering/

Distributed plasticity approach for the nonlinear structural assessment of offshore wind turbine

Thanh-Tuan Tran [a, b], Mosaruf Hussan [c], Dookie Kim [d, *], Phu-Cuong Nguyen [e]

[a] Institute of Offshore Wind Energy, Kunsan National University, 558 Daehak-ro, Gunsan-si, Jeollabuk-do, Republic of Korea
[b] Faculty of Technology and Technique, Quy Nhon University, Binh Dinh province, Viet Nam
[c] Department of Civil and Environmental Engineering, Kunsan National University, 558 Daehak-ro, Gunsan-si, Jeollabuk-do, Republic of Korea
[d] Department of Civil and Environmental Engineering, Kongju National University, 1223-24, Cheonan-daero, Seobuk-gu, Cheonan, Chungcheongnam-do, Republic of Korea
[e] Faculty of Civil Engineering, Ho Chi Minh City Open University, Viet Nam

ARTICLE INFO

Article history:
Received 14 November 2019
Received in revised form
9 August 2020
Accepted 13 September 2020

Keywords:
Offshore wind turbine
Incident angle
Fragility curve
Fiber section
Incremental dynamic analysis
Damage state

ABSTRACT

This study provides an insight of the nonlinear behavior of the Offshore Wind Turbine (OWT) structure using the distributed plasticity approach. The fiber section beam-column element is applied to construct the finite element model. The accuracy of the proposed model is verified using linear analysis via the comparison of the dynamic characteristics. For collapse risk assessment of OWT, the nonlinear effects considering the earthquake Incident Angle (IA) have been evaluated first. Then, the Incremental Dynamic Analysis (IDA) has been executed using a set of 20 near-fault records. Lastly, fragility curves are developed to evaluate the vulnerability of structures for different limit states. Attained results justify the accuracy of the proposed approach for the structural response against the ground motions and other environmental loads. It indicates that effects of static wind and wave loads along with the earthquake loads should be considered during the risk assessment of the OWT structure.

1. Introduction

Wind turbines are one of the potential energy resources all over the world. Many researchers have focused on the study of the Offshore Wind Turbine (OWT) (Ahn et al., 2017; Pham and Shin, 2019; Sharmin et al., 2017b; Zuo et al., 2017). The horizontal axis wind turbine blade model has been constructed based on aerodynamics and produced FAST software for real-time simulation of wind turbine operational status (Jonkman, 2009). Based on vibration control and the structural response of OWT, lots of research has been performed (Hussan et al., 2018; Sharmin et al., 2017b; Tran et al., 2019). There are many reasons for the risks of OWT, which depends on environmental conditions such as various loads, ground conditions, etc. Many researchers have been done and invented previously to investigate the seismic analysis of OWT such as seismic analysis in the time domain (Meng et al., 2019; Witcher, 2005), seismic fragility analysis (Kim et al., 2014), seismic response due to earthquakes and wind loading (Kjørlaug, 2014), FAST simulation of the wind turbine seismic response (Prowell et al., 2009) and so on. Besides the seismic load, the wind and wave loads are the two important loads, which can overreach damage states and failure of the structure (Dueñas-Osorio and Basu, 2008; Feyzollahzadeh et al., 2016; Lai et al., 2016; Li et al., 2018; Murtagh et al., 2005). For example, the dynamic behavior of jacket substructure under extreme environmental conditions has been conducted by Lai et al. (2016). Similar work has been carried out by Feyzollahzadeh et al. (2016) to evaluate the wind load response of offshore wind supported by a monopile foundation. In this research, the static wind and wave loads with dynamic seismic loads are considered for evaluating the nonlinear dynamic responses of OWT.

Nonlinear behaviors depend on the description of nonlinear modeling of structure in the numerical model. The discrete finite element model is the best comparison between the simplicity and accuracy of nonlinear analysis that can be classified into two categories: the lumped and the distributed plasticity models (Clough and Benuska, 1967; Taucer, 1991). The lumped plasticity approach proposed by Clough and Benuska (1967) employs the simplicity of

* Corresponding author.
E-mail addresses: tranthanhtuan@kunsan.ac.kr, tranthanhtuan@hotmail.com.vn (T.-T. Tran), razib.mosaruf@kunsan.ac.kr (M. Hussan), kim2kie@kongju.ac.kr (D. Kim), cuong.pn@ou.edu.vn (P.-C. Nguyen).
Peer review under responsibility of Society of Naval Architects of Korea.

https://doi.org/10.1016/j.ijnaoe.2020.09.003

the plastic hinge concept of separating a line element into elastic and inelastic components. Elastic and inelastic behaviors are considered by using two components acting in parallel. So, the distributed plasticity model is introduced in this study to get a better assessment of the structure. The model allows yielding to occur at any location along the element section. A plasticity analysis process of plane steel frames using a displacement-based finite element has been investigated by Nguyen and Kim (2018). Recently, the effect of structural nonlinearity of OWT has been executed through the plastic hinge model by Sharmin et al. (2017a). In this study, the nonlinear effects of OWT have been evaluated as a materially nonlinear model by using the fiber-based modeling approach for the annular section of OWT.

In seismic design, the earthquake motions are considered in principal directions of the structure. However, the main direction of the earthquake and principal axes of the structure are not identical, and the direction of ground motion causes different structural responses, according to Penzien and Watabe (1974). Therefore, the structure should be resistant under different excitation angles of the earthquake to get an accurate estimation of structural execution and damage (Kojima and Takewaki, 2016, 2015). A method has been introduced by Wilson and Butto (Wilson and Button, 1982) to estimate the angle of incidence of earthquakes. Smeby and Kiureghian (Smeby and der Kiureghian, 1985) have presented an explicit numerical model to estimate the critical angle of incidence apprehending horizontal components of ground motion. The essential of Incident Angle (IA) has been conducted for lots of structures such as asymmetry building (Nguyen and Kim, 2017; Van Tu and Kim, 2013), nuclear power plant (Tran et al., 2018), etc. The present study has been conducted based on the earthquake incidence of OWT under the effect of structural nonlinearity, which has been rarely done in the OWT field.

Incremental Dynamic Analysis (IDA) has been recently developed as an efficient approach for estimating the seismic demand on structure (Tran et al., 2019; Vamvatsikos and Cornell, 2002). IDA is also used to evaluate the seismic fragility for structure (Vamvatsikos and Cornell, 2002), such as for building (Ellingwood et al., 2007; Tran et al., 2017), bridges (Zhang and Huo, 2009), nuclear equipment (Cao et al., 2019; Salman et al., 2020) or steel structures. Fragility analysis is defined as a conditional probability of failure at intensity level when the seismic response of the structure exceeds the failure capacity (Shinozuka et al., 2000). This paper develops a fragility curve for OWT structure from the IDA method, where there is no need to perform analysis up to collapse intensity measure (Baker, 2015).

The present research investigates the dynamic behavior of jacket supported OWT structures. The nonlinear response of the structure is considered using the distributed plasticity approach. The behavior of the structure has been evaluated considering the multi-component seismic excitations oriented by the IA. For this purpose, the computer program VC4OWT (Vibration Control of Offshore Wind Turbine), written in MATLAB, has been developed (Tran et al., 2019). The program is used to determine the structural responses (i.e., displacement, rotation) of National Renewable Energy Laboratory (NREL) 5-MW OWT subjected to seismic excitations. Finally, fragility analysis has been done to examine the vulnerability and risk assessment of the structure by using IDA under two different load patterns with different limit states.

2. Ground motion selection and earthquake incidence angle

2.1. Ground motion selection

Prior to conducting a nonlinear response history analysis, the ground motion records must be chosen. In Table 1, the relevant earthquakes with basic information are listed. All of the 20 near-fault records and data are downloaded from the Pacific Earthquake Engineering Research (PEER) Ground Motion Databases (Ancheta et al., 2012), which is one of the most comprehensive databases of earthquake records and data sets available in the world. The closest distance-to-ruptured area (denoted as R_{RUP}) range from 0.34 km to 15.23 km. Meanwhile, the range of magnitudes is between 6.5 and 7.5, which shows their relationship in Fig. 1(a). There is no specific consideration of the type of faulting or the characteristic to consider the spectral shape, epsilon. The results of PGA values are from 0.27 g to 0.86 g, and the resulting response spectra are shown in Fig. 1(b).

2.2. Earthquake incidence angle on seismic performance analysis

For a structure subjected to the ground motion for a pair of given ground motion, one of the two horizontal components is classified as either a major component and a minor component based on its PGA value. The one with the highest PGA corresponding to the major component, while the other is a minor component. Therefore, x and y are called the axes of the structure. The major (p axis)

Table 1
Details of the ground motion records.

Earthquake Name	Year	Station Name	R_{RUP} (km)	PGA_1 (g)	PGA_2 (g)
Tabas_Iran	1978	Tabas	2.05	0.854	0.862
Imperial Valley-06	1979	Aeropuerto Mexicali	0.34	0.307	0.271
Imperial Valley-06	1979	El Centro Array #4	7.05	0.484	0.370
Imperial Valley-06	1979	El Centro Array #5	3.95	0.529	0.383
Imperial Valley-06	1979	El Centro Array #6	1.35	0.447	0.449
Loma Prieta	1989	Capitola	15.23	0.511	0.439
Loma Prieta	1989	Gilroy Array #2	11.07	0.370	0.323
Northridge-01	1994	Canoga Park - Topanga Can	14.7	0.358	0.392
Northridge-01	1994	Northridge - 17,645 Saticoy St	12.09	0.341	0.459
Northridge-01	1994	Sun Valley - Roscoe Blvd	10.05	0.277	0.447
Kobe_ Japan	1995	KJMA	0.96	0.834	0.630
Kobe_ Japan	1995	Takatori	1.47	0.618	0.671
San Fernando	1971	Pacoima Dam (upper left abut)	1.81	0.854	0.862
Superstition Hills-02	1987	Parachute Test Site	0.95	0.307	0.271
Tottori_ Japan	2000	SMN015	9.12	0.484	0.370
San Simeon_ CA	2003	Cambria - Hwy 1 Caltrans Bridge	7.25	0.529	0.383
Niigata_ Japan	2004	NIG017	12.81	0.447	0.449
Chuetsu-oki_ Japan	2007	Joetsu Kakizakiku Kakizaki	11.94	0.511	0.439
Iwate_ Japan	2008	Mizusawaku Interior O ganecho	7.85	0.370	0.323
Darfield_ New Zealand	2010	LRSC	12.52	0.358	0.392

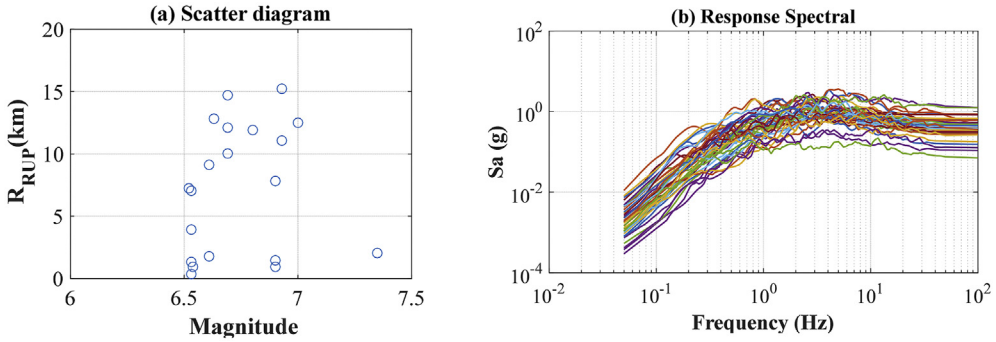

Fig. 1. Details of input ground motions.

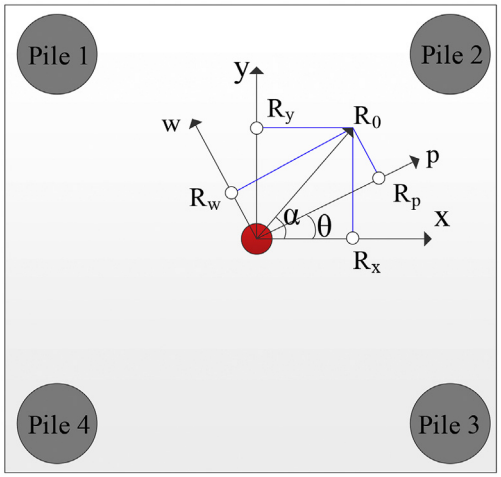

Fig. 2. Definition of incident angle.

and minor (w axis) components are additionally rotated θ away from the x -axis, as shown in Fig. 2. Moreover, the angle between x and direction p, which is the incidence angle, is called θ, while the angle between the x -axis and the direction of maximum displacement is called α.

In Fig. 2, R_x and R_y are represented as response quantities along the x and y excitations, respectively (Athanatopoulou, 2005; Tran et al., 2018). Therefore, R_0 is denoted the resultant response of R_x and R_y, which satisfy the following Eqs. (1) and (2):

$$R_0(t) = R_x(t)\cos\alpha(t) + R_y(t)\sin\alpha(t) \tag{1}$$

$$\alpha(t) = \tan^{-1}\left(\frac{R_y(t)}{R_x(t)}\right) \tag{2}$$

Here, $\alpha(t)$ is the angle between R_0 and R_x, which is revealed as the time-dependent variable. The response quantities of rotated components R_p and R_w are defined as Eqs. (3) and (4):

$$R_p(\theta, t) = R_0(t)\cos[\alpha(t) - \theta] \tag{3}$$

$$R_w(\theta, t) = R_0(t)\sin[\alpha(t) - \theta] \tag{4}$$

3. Structural modeling

3.1. Model description

In this study, the adopted structural model is a 5 MW OC4 jacket supported OWT. This benchmark OWT has been developed following by the National Renewable Energy Laboratory (NREL) (Jonkman et al., 2009), as shown in Fig. 3. The full model consists of RNA, tower, TP, jacket structure and a circular foundation (monopile below the mudline). The general properties of the OWT structure are summarized in Table 2. The platform is considered as fixed to eliminate the influence of the foundation. The total height of the structure is 138 m, where tower and jacket heights are 68 m and 70 m, respectively. The jacket support structure consists of 64 nodes and 112 elements, which are subjected to the wave nodal loads. The tower is composed of the combination of 9 elements. The interface nodes of the jacket rigidly connected to the Transition Piece (TP). TP is represented as a density filling a rectangular body with 1807 kg/m^3 of mass density. Young's and shear modulus and Poisson's ratio of the TP are 2.06×10^3 GPa, 0.79×10^3 GPa and 0.18, respectively. The rotor nacelle assembly (RNA) is assumed as rigid bodies and its mass is considered as lumped mass at the top of the tower.

3.2. Load considerations

The support structure used in this study is based on the design for the offshore code collaboration continuation (OC4) project at a water depth of 50 m and water density of 1025 kg/m^3 (Song et al., 2013; Vemula et al., 2010). The environmental condition, including the wind and wave loads, as shown in Table 3, have been applied to the tower and the jacket nodes as external nodal forces and moments.

The wind forces on a unit height of the tower are expressed by f, the base shear and base overturning moment can be given by Eqs. (5) and (6).

$$F = \int_0^H f(z)dz = \int_0^H \frac{1}{2}\rho_{air}U(z)^2 C_P D(z)dz \tag{5}$$

$$M = \int_0^H f(z)zdz = \int_0^H \frac{1}{2}\rho_{air}U(z)^2 C_P D(z)zdz \tag{6}$$

where H is the height from the ground to the center of the hub, ρ_{air} is the air density, $U(z)$ is wind speed corresponding with the height z, C_D is the drag coefficient for the tower, D and z are the diameter and height of the tower, respectively.

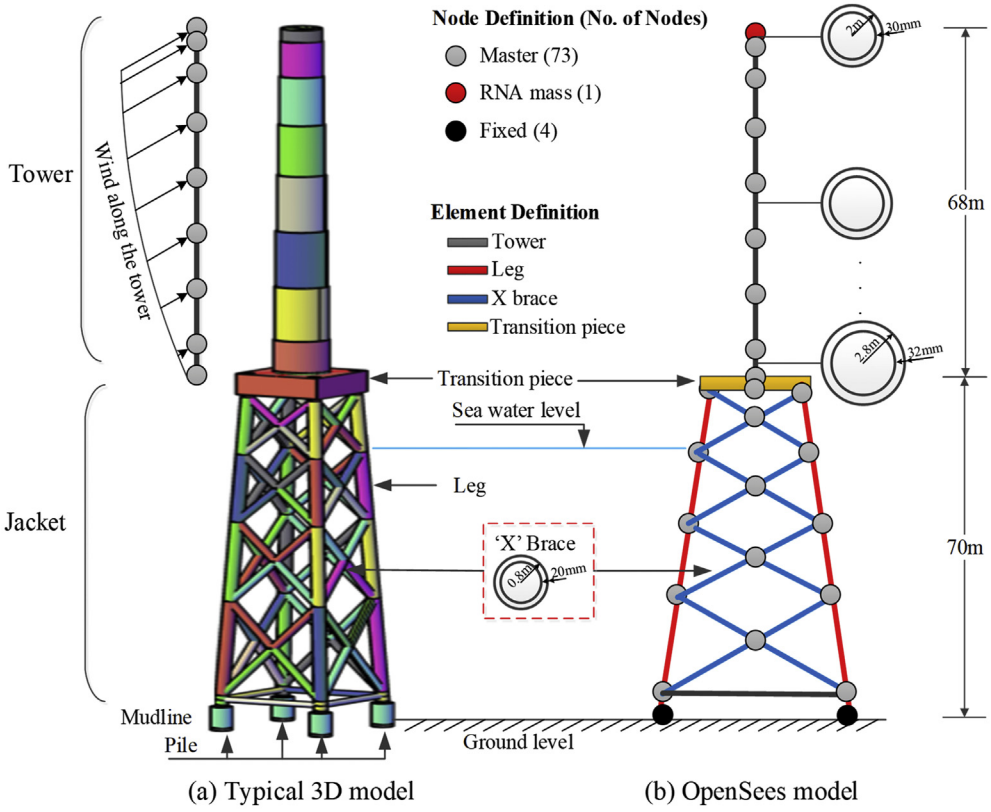

Fig. 3. Model of jacket supported OWT.

Table 2
Properties of the jacket supported OWT.

Parameter	Description	Unit	Value
	Platform type	–	Fixed platform
	TP dimension	m^3	$9.6 \times 9.6 \times 4$ and 666×10^3
m_{TP}	TP mass	kg	666×10^3
m_{RNA}	RNA mass	kg	350×10^3
m_{jacket}	Jacket mass	kg	655.83×10^3
m_{OWT}	Total OWT mass	kg	1.9018×10^6
$d(t)_{br}$	Diameter (thickness) of braces (Jacket and Mud)	m	0.8 (0.02)
$d(t)_{pl}$	Diameter (thickness) of pile	m	2.08 (0.49) (upper), 2.08 (0.069) (lower)
h_{hub}	Hub height	m	90

Table 3
Environmental conditions of the reference site (Jonkman et al., 2009).

Description	Symbol	Value	Unit
Wind			
Reference height for horizontal wind speed	H_{ref}	90	m
Wind speed at reference height	V_{ref}	5	m/s
Wave			
Water depth	d_{MSL}	50.0	m
Significant wave height	H_S	8	m
Period	T_S	10	s

Wave forces on the slender structural member, such as a cylinder submerged in water, can be predicted by Morison's equation (7).

$$dF = dF_M + dF_D = C_M \rho \pi \frac{D^2}{4} \dot{v} dz + C_D \rho \frac{D}{2} |v| v dz \quad (7)$$

where the first term is an inertia force and the second term is a drag force, C_D and C_M are drag and mass coefficient, respectively. D and A are the diameter and cross-section area of the cylinder, respectively, ρ is the density of water, $\dot{v}$ and v are fluid particle (waves and/or current) acceleration and velocity of the water. Details of diameter and calculated cross-section area are taken from Table 4. In this study, the wind and wave loads have been getting from FAST, and they are applied as a static force on the tower and jacket nodes.

3.3. Modeling of the nonlinear behavior

3.3.1. Plasticity approaches

Over the past years, there are several approaches used to simulate the nonlinear behavior of frame structure due to earthquake loadings. These approaches can be classified into two main categories (Fig. 4): Concentrated Plasticity (CP) and Distributed Plasticity (DP) (Taucer, 1991). These approaches assume that the nonlinear behavior can occur at the end of the structural element (CP) or along the element and over the element cross section (DP).

Table 4
Annular section details of OWT.

Jacket Item	Br1[a]	Br2	Br3	Br4	Br5	Br6
Diameter (m)	0.800	1.200	1.200	1.200	2.080	2.080
Thickness (m)	0.020	0.050	0.035	0.040	0.491	0.060

Tower Item	T1[a]	T2	T3	T4	T5	T6	T7	T8	T9
Diameter (m)	5.600	5.557	5.318	5.082	4.800	4.565	4.329	4.118	4.000
Thickness (m)	0.032	0.032	0.030	0.028	0.024	0.022	0.020	0.030	0.030

[a] Br1: Bracing 1, T1 = Tower 1.

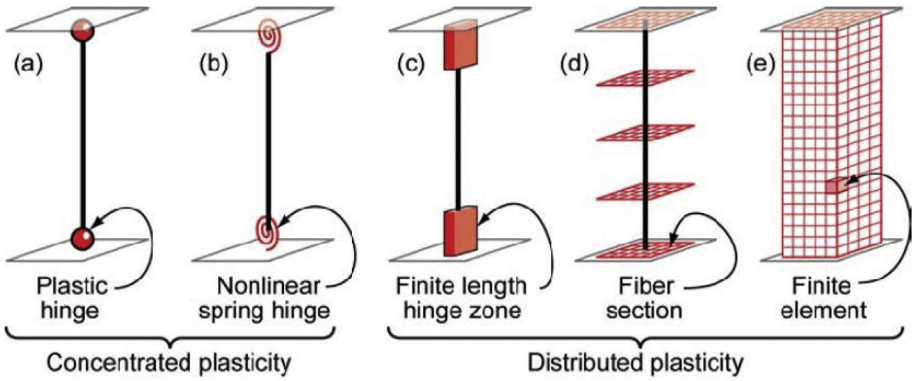

Fig. 4. Classification of the models (Andreotti and Lai, 2017).

3.3.2. Modeling with distributed approach for OWT

In this study, the OWT has been carried out in OpenSees using the distributed plasticity approach. This software is used as it can effectively reduce the computational time compared to other software (ANSYS, ABAQUS). The input parameters required for a distributed plasticity element consist of the number of integration points, number of sub-elements, and the definition of a fiber-based section to be applied to each integration point. A schematic of the distributed plasticity element used for the analyses is shown in Fig. 5. Two nodes I and J are located at the end of the element. The integration points divide elements into sub-elements. The local coordinate of sub-element XYZ is shown in Fig. 5. The X-axis is along the longitudinal axis of sub-element, where Y and Z axes are major and minor principal axes of the cross-section. The material nonlinearity is considered by the relationship of stress-strain of each fiber on the cross-section of the sub-element. In this approach, the nonlinearity in the distributed plasticity model can occur at any fiber of cross-section.

The structure is modeled using nonlinear beam-column and divided into several sub-elements along the length of the member. Each element is divided into many small fibers. The cross-section of this element is constructed using the fiber section approach with annular section. Details of the annular section are listed in Table 3. The number of divisions across the thickness and along of the circle is 8 and 36, respectively. The Steel 01 material model with the elastic modulus of 2.1×10^{11} N/m^2, the yield stress of 3.25×10^8 N/m^2 and strain hardening bilinear behavior 3% is used. The section aggregator command is added to the fiber section for showing the shear deformation behavior of the section. In short, this materially nonlinear model response with fiber section is expected to illustrate the real behavior of OWT. A materially nonlinear model can analyze high-rise structure like OWT subjected to earthquake forces within the inelastic range.

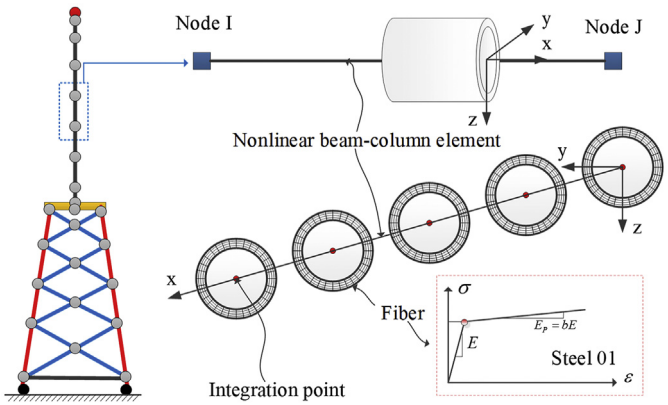

Fig. 5. Distributed plasticity element.

3.4. Verification and validation

In order to validate the finite element model, the modal analysis is performed and the frequencies are compared with the results generated in other works. The natural frequencies from the dynamic analysis of ANSYS (Nuta, 2010) and FAST (Jonkman et al., 2009) are conducted. As observed, the results show a good agreement with OpenSees numerical results.

The models of OWT with the fiber-section model and nonlinear beam-column element are performed. The frequencies of structures are listed in Table 5. This observation leads to the conclusion that the effects of element inelastic behavior have great importance to jacket supported structure. The nonlinearity may occur in any element section. The maximum responses are determined at first and second mode frequencies, they are 0.231 Hz and 0.837 Hz, respectively, which can be explained more detail in Fig. 6 with a frequency response curve of the tower top.

Table 5
The natural frequency of the OWT structure (Hz).

Mode	Description	ANSYS	FAST	OpenSees	
				Linear	Nonlinear
1	1st Fore-Aft mode	0.291	0.319	0.3273	0.231
2	1st Side-Side mode	0.292	0.319	0.3273	0.231
3	2nd Fore-Aft mode	1.317	1.194	1.1743	0.837
4	2nd Side-Side mode	1.321	1.194	1.1743	0.837

A Fourier transform is executed to obtain the frequency spectrum for the results of the top acceleration over time. This is performed to verify the nonlinear model with fiber section and assert how the natural frequencies of the OWT structure change due to the nonlinear effects. Here, two earthquakes (i.e., Tabas (1978), and Northridge (1994)) are used randomly for the idealization of OWT model. Fig. 6 illustrates the frequency response curve of the tower top acceleration.

Based on Fig. 6, the position of the maximum peaks can be found at first (0.231 Hz) and second (0.837 Hz) natural frequencies for nonlinear analysis. This trend is also identical for linear analysis with the corresponding values of 0.327 Hz and 1.178 Hz. The frequency reposne curves shift leftward with nonlinear case, which demonstrates a decrease in natural frequencies. This can be explained due to the decrease of stiffness since nonlinearity provides less stability of the structure due to the reduced stiffness.

4. Influence of earthquake incidence on the seismic responses of OWT

To examine the response of fiber section to the response of the structure, five records have been selected from 20 above earthquakes. These are Tabas_Iran (Tabas), Imperial Valley (El Centro Array #4), Loma Prieta (Capitola), Northridge-01 (Canoga Park – Topanga Can) and Kobe_Japan (KJMA). All of those records are applied that vary from 0 to 360°, with an interval of 15° to show their effects on engineering demand parameters (EDPs). The maximum displacement and rotation at the tower top are shown as EDPs.

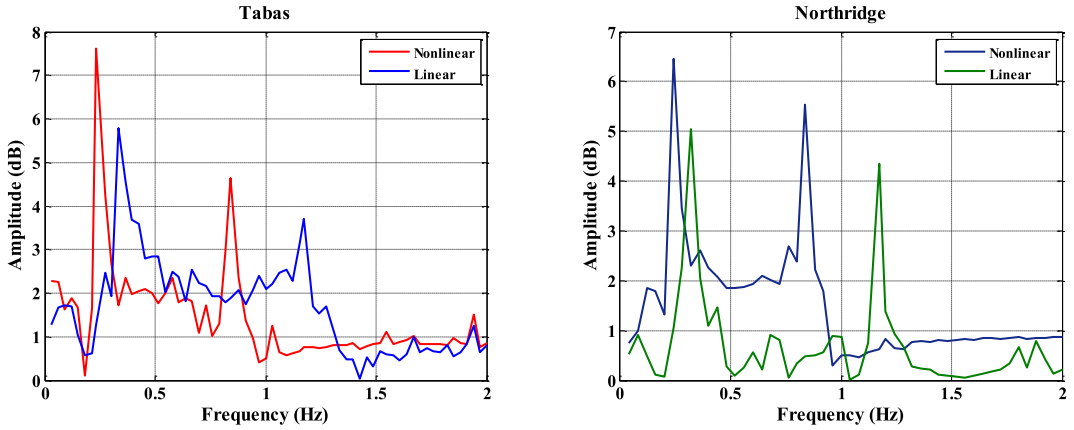

Fig. 6. Frequency response curves.

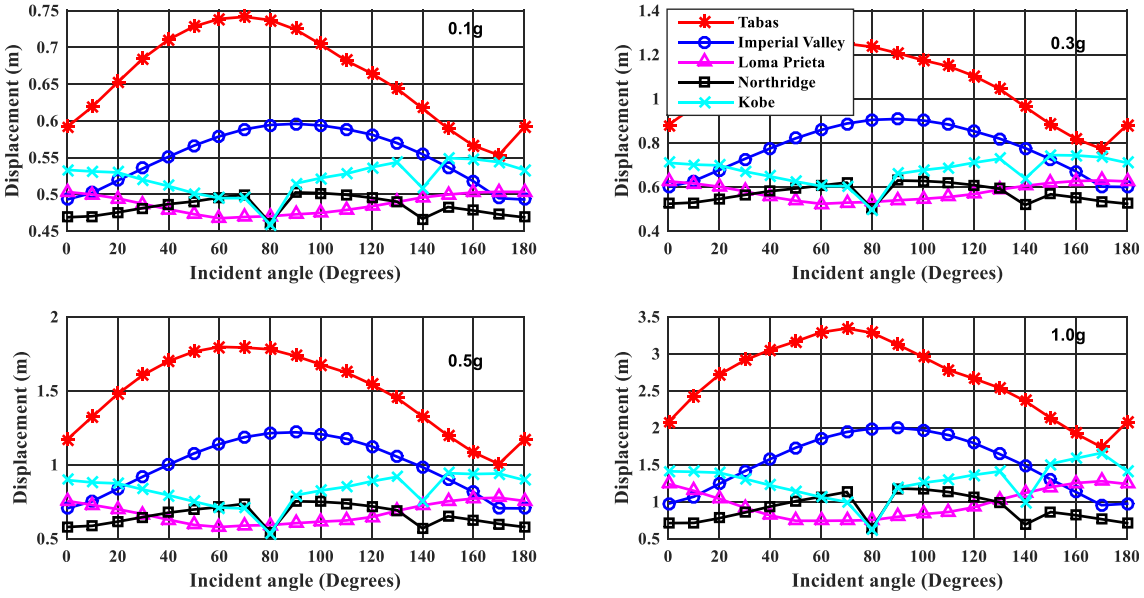

Fig. 7. Displacement response assessment considering earthquake incidence.

4.1. Top displacement and rotation

The maximum displacement and rotation under the different incident angles of ground motion are shown in Fig. 7 and Fig. 8, respectively. As the responses from 190 to 360° coincide with the result in the range of 0 and 180°, so the author only shows for later value. It is obvious that due to the variation of the incident angle for each ground motion, the obtained maximum response is different from each other response of the structure. The maximum displacement at the top of the tower for the case of Imperial Valley changes from 0.551 m to 0.908 m for the 0.3 g PGA, while in case of 1.0 g intensity level the maximum displacement is 0.813 m and 1.997 m, respectively. For the maximum rotation at the tower top, these values vary 0.458 ° and 0.749 ° for 0.3 g intensity level, the results increase around 2 times for 1.0 g PGA, they are 0.752 ° and 1.553 °. A second remarkable point is that at the angle of 80 ° and 140 ° the structural responses drop suddenly to get the minimum response with the different incident angle. This leads to the conclusion that the orthogonal directions of earthquakes should be reviewed in the principal directions of the structure (Penzien and Watabe, 1974), it can be decreased at some angles and increased at other angles.

The boxplot illustrated in Fig. 9 shows the relative error of displacement and rotation at the tower top for 1.0 g PGA intensity level. Comparison the bottom and top values of the boxes that define the 25% and 75% percentiles shows that the relative displacement and rotation for the Imperial Valley earthquake is the largest one while for the Kobe earthquake is shown the smallest one compared to the rest of the earthquakes.

The maximum and minimum values along with the mean value and the Coefficient of Variation (COV) of the maximum displacement and rotation at the tower top considering the variation of incident angle are given in Appendix. The range of intensity measure of PGA is also shown in the table. It is obvious that the critical incident angle varies for the intensity level of ground motions and depend on the damage measures as displacement and rotation. This leads to the conclusion that it is hard to predict the critical incident angle of the structure when changing the intensity level of ground motion.

The COV of displacement and rotation are illustrated in Fig. 10. It can be seen that the COV changes with the intensity level and the ground motions. The variations of response, including the COV of top displacement and rotation increase gradually from the 0.1 g–1.0 g intensity level.

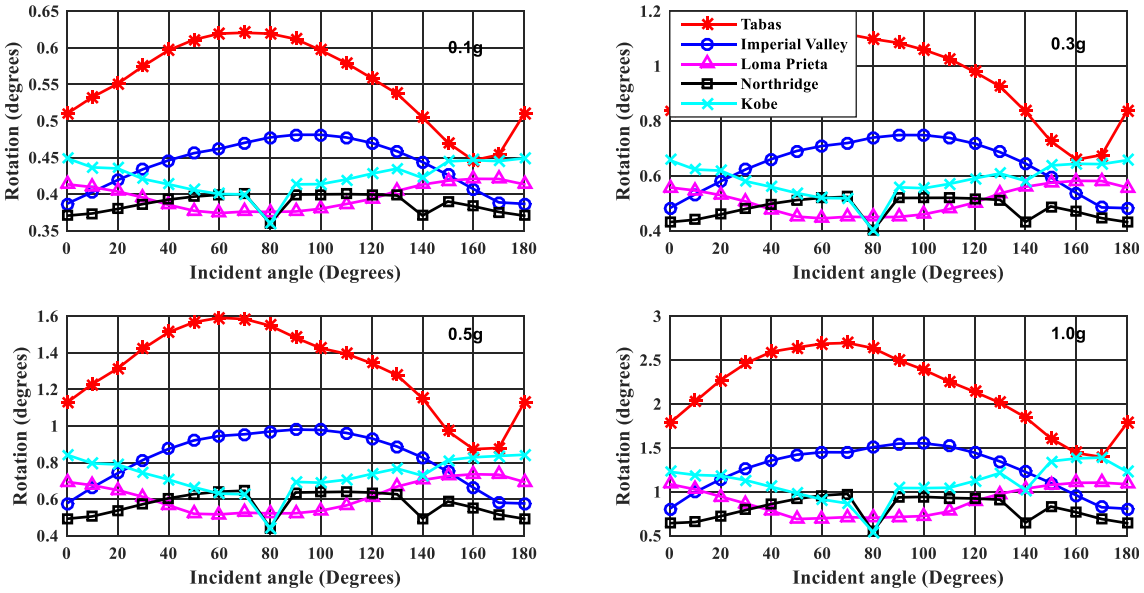

Fig. 8. Rotational response assessment considering earthquake incidence.

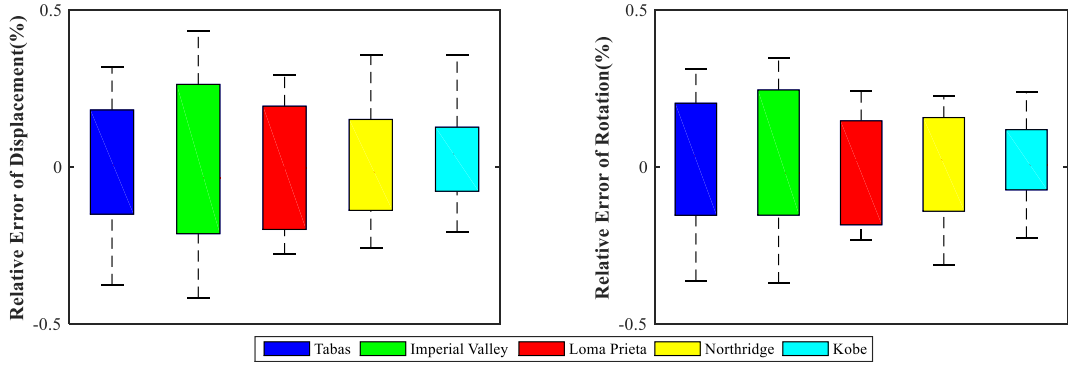

Fig. 9. Relative errors of displacement and rotation of earthquakes.

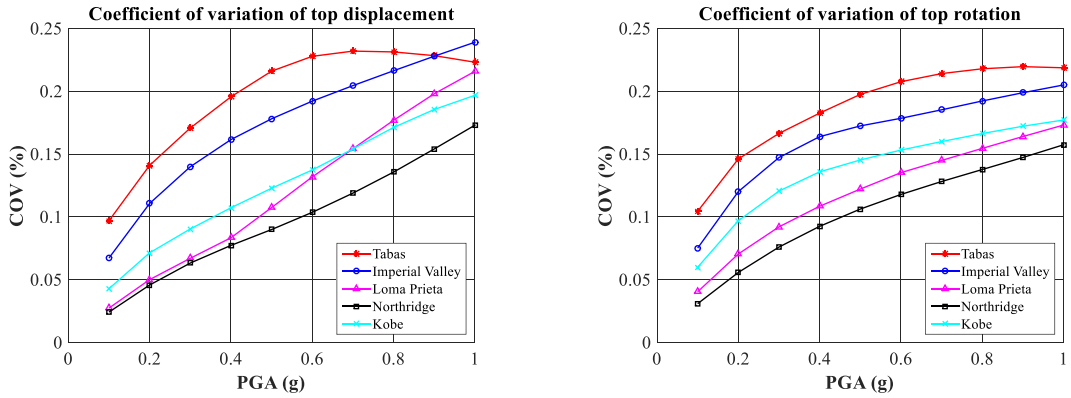

Fig. 10. COV of top displacement and rotation under seismic excitations.

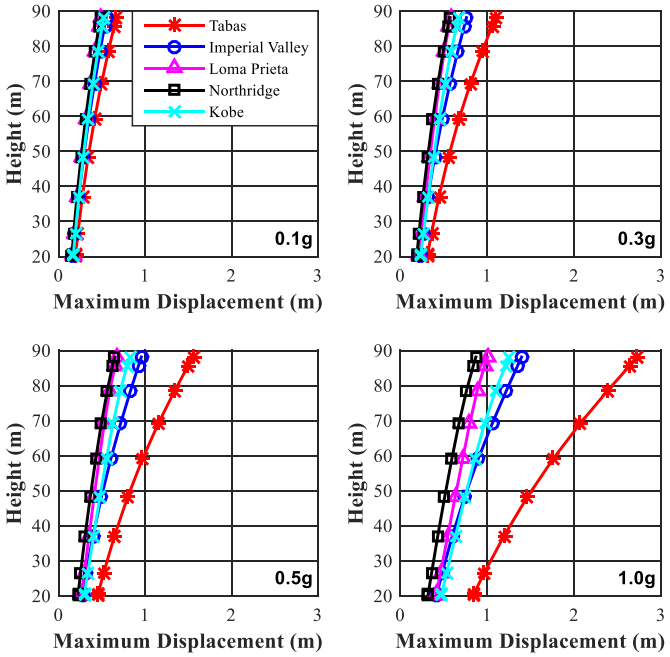

Fig. 11. Lateral displacement assessment.

4.2. Lateral displacement

Fig. 11 presents the mean lateral displacements under ground motions at the different tower height respect to intensity levels. The variation of lateral displacements increases and distinguishes clearly at higher intensity level under different records. By increasing the intensity of earthquakes, the displacement is also increased from a linear to nonlinear range.

As shown in Fig. 12, the maximum displacement and rotation at the tower top rise with the intensity level when PGA value changes to 1.0 g. The response of structure increases linearly and the maximum displacement and rotation at the tower top are 2.72 m and 2.19 ° for Tabas record with a PGA of 1 g.

5. Risk assessment using fragility curve

5.1. Methodology

Fragility curve is a statistical tool, which describes the probability of exceeding a given Damage State (DS) as a function of an engineering demand parameter that represents different intensity levels. The cumulative distribution function of a lognormal distribution is used to define a fragility function (Cao et al., 2019; Shinozuka et al., 2000).

$$P(x) = \Phi\left(\frac{\ln\left(\frac{x}{\theta}\right)}{\beta}\right) \tag{8}$$

where P is the probability that a GM with $PGA = x$, will cause the structure to collapse, θ and β are the median and the standard deviation of the intensity measures, respectively. $\Phi()$ is the standard normal Cumulative Distribution Function (CDF).

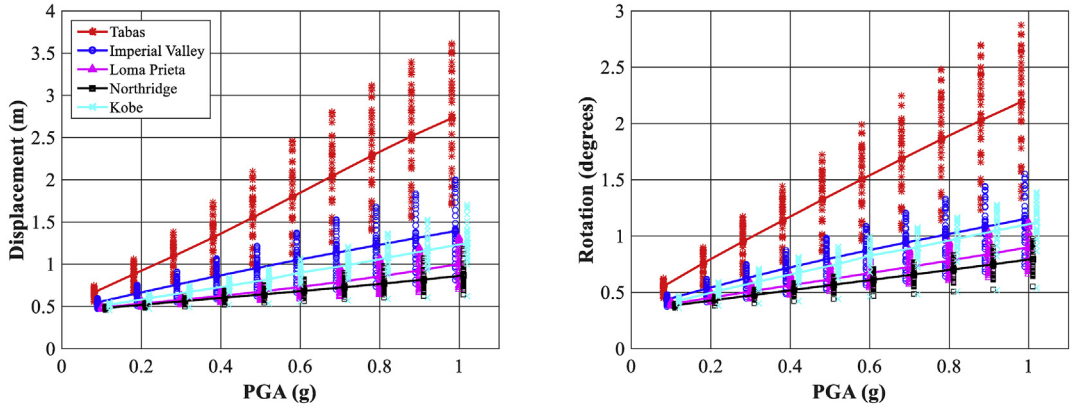

Fig. 12. Maximum displacement and rotation at the tower top under seismic excitations.

Assuming that the PGA $= IM_j$ for each ground motion is independent, the likelihood function of the entire data set is given by

$$Likelihood = \left(\prod_{j=1}^{m} \Phi\left(\frac{\ln(IM_j/\theta)}{\beta}\right)\right)\left(1-\Phi\left(\frac{\ln(IM_{max}/\theta)}{\beta}\right)\right)^{n-m} \tag{9}$$

where m is the number of PGA levels and Π denotes the product over all levels. The fragility function parameters θ and β are obtained by maximizing the likelihood function (Baker, 2015).

$$\{\hat{\theta},\hat{\beta}\} = \underset{\theta,\beta}{\operatorname{argmax}} \sum_{j=1}^{m}\left\{ \ln\varphi\left(\frac{\ln(IM_i/\theta)}{\beta}\right) + (n-m)\ln \left(1-\Phi\left(\frac{\ln(IM_{max}/\theta)}{\beta}\right)\right)\right\} \tag{10}$$

5.2. Damage states

To estimate the fragility curves of the OWT structure, two limit states are defined from the demand parameters of the OWT. The damage states (DSs) applied to the wind turbine are shown in Table 6. The two DSs in this study is related to the maximum displacement and rotation at the tower top. The DS1 is defined, when the displacement comes to 1.25% height of the tower proposed by Asareh et al. (2016, 2015). The rotation value of 2.5 °at tower top is employed for DS2.

5.3. Incremental dynamic analysis

The nonlinear time history analyses are conducted on the model. The risk assessment of OWT is performed using the VC4OWT (Tran et al., 2019). The schematic description of the process is depicted in Fig. 13. The step-by-step of the methodology is as follows:

Table 6
Damage states considered for fragility analysis (Asareh et al., 2016, 2015).

Damage state	Critical Response	Description
DS1	1.73 m	1.25% H top displacement
DS2	2.5°	2.5° rotation at tower top

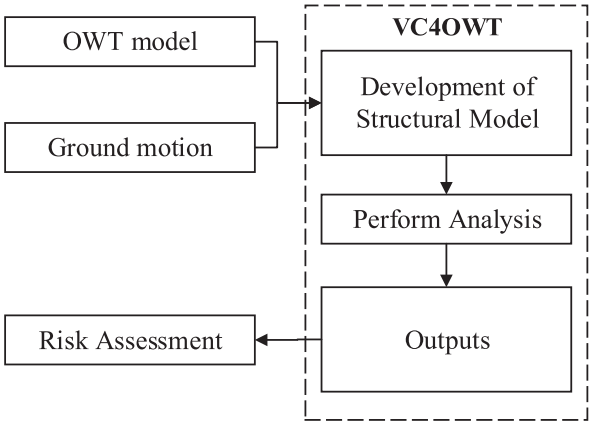

Fig. 13. Flowchart of the software VC4OWT.

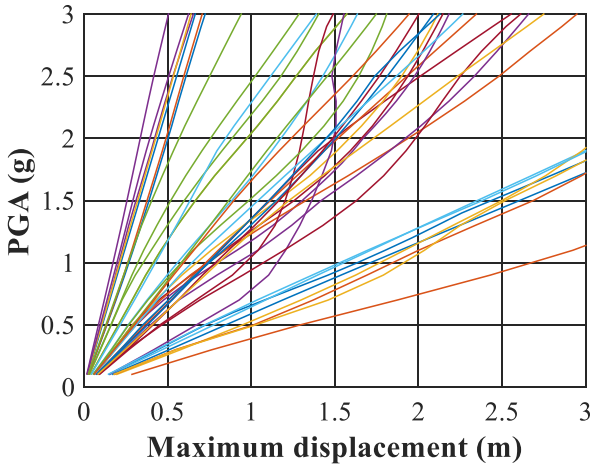

Fig. 14. IDA curves for the suite of ground motions.

- Step 1: preparing the input files for analysis: the OWT data and ground motions
- Step 2: the structural model is developed based on the input file. Time history analysis is conducted for each ground motion. Finally, the response is obtained.
- Step 3: developing the fragility curves based on the obtained outcomes in Step 2.

The IDA curves are generated from the nonlinear time history analysis results, which is shown in Fig. 14. The IDA analyses have been considered for the maximum displacement as the damage measure and the PGA as the intensity measure for 20 records in two horizontal directions. An increment of 0.05 g in PGA is selected to capture the yield and collapse capacity of the structure with reasonable sensitivity. The IDA curves display the full range of behavior, showing quite large record-to-record variability. Generally, the shape of the IDA curve is different for each ground motion. Using the selected ground motions, 40 IDA curves are generated for each direction (i.e., 20 for x-direction and 20 for y-direction). It can be predicted that when increasing the intensity levels, the maximum displacement rises, which shows the failure of the structure.

5.4. Fragility curves

Fig. 15 represents the fragility curves of structure for (a) individual seismic load and (b) wind, wave, and seismic loads together. The median fragility curves, as well as the 95% and 5% confidence intervals, are shown. Based on the obtained results, the median PGA (θ) and lognormal standard deviation (β) of the fragility curve change due to the wind, wave, and seismic load. Note that for both damage states, the median PGA for a seismic load case only is higher than that exhibited by all loads. The fragility curve for the individual seismic load in Fig. 15(a) showing the θ for first and second damage states are 2.417 g and 3.022 g, respectively. However, when considering the wind and wave loads, these values change more obviously. These decreases in median PGA are 1.533 g and 2.794 g for DS1 and DS2, respectively. This can be explained that for a seismic load case only are considered, the wind and wave loads have significant effects on the nonlinear behavior of OWT structure. In addition, when applying all loads (Fig. 15(b)), a value 2 g of ground motion is exposed, the probabilities of exceeding are approximately 70% and 20% for DS1 and DS2, respectively. Moreover, the probabilities of the damage states are very low, when the

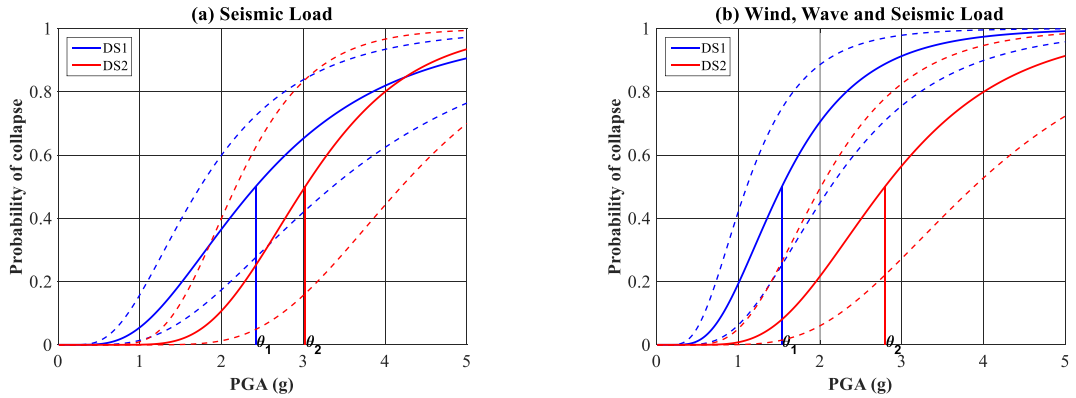

Fig. 15. Comparison of fragility: median curves (solid lines) and 95% and 5% confidence intervals (dash lines).

Table 7
Median and dispersion value of fragility function.

Loads	DS1		DS2	
	θ	β	θ	β
Seismic	2.417	0.553	3.022	0.333
Wind, wave and seismic	1.533	0.494	2.794	0.427

PGA value is smaller than 0.5 g and 1.0 g, respectively, for DS1 along with DS2. When the PGA rises beyond 0.5 g in the DS1, the fragility curve is increased quickly and shown almost 100% at 5 g. The corresponding median and dispersion values of the fragility curve are shown in Table 7. It is observed from the table that the lognormal standard deviation of DS1 is larger than that of DS2.

Based on the summarized results shown in Fig. 15, the fragility curves for seismic load only and combined wind, wave, and seismic loads showed a different trend relating to different load effects. For a seismic load case only, the probability of exceeding of DS2 is higher than DS1 when the PGA is more than 4 g. Moreover, applying the wind and wave loads together with the seismic load will expose a lager response. This is caused by the governance of static loads in behavior of OWT structural. This observation leads to the conclusion that the interaction of the wind, wave, and seismic loads has a significant effect on OWT structure, which is required for further investigation to get the precise outcome of the structure.

6. Conclusions

A nonlinear finite element model of OWT is developed in OpenSees platform using the nonlinear beam-column element with fiber section model for evaluating the structure behavior. The response of OWT considering earthquake incidence is evaluated. The static wind and wave loads are considered for evaluating the response structure. The results are summarized as follows:

- The influence of nonlinear model with the fiber section element to both frequency and structure behavior is noticeable. Nonlinear behavior under the anomalous structures shows the extreme behavior rather than ordinary structures while the structures subjected to earthquake incidence.
- Fragility curve of the OWT structure has been developed using the incremental dynamic analysis. The different damage states based on the previous research analyses outcomes are applied for plotting the fragility curve. The maximum displacement and rotation at the tower top as engineering demand parameters corresponding to the damage states are introduced.
- By considering the effectiveness of nonlinear modeling of structure with the distributed plasticity approach, an enhanced model for OWT is developed to obtain more realistic simulation. The proposed model provides better predictions on the structural response.
- For implementing the collapse risk assessment of OWT, the results indicate that the probability of exceeding is mainly governed by the effect of static load conditions. When static wind and wave loads are applied, the probability of exceeding increased as compared to the case of seismic load only.

Dynamic wind and wave loads together with the seismic loads instead of static environmental loads may be needed as further research.

Declaration of competing interest

The authors declare that they have no known competing financial interests or personal relationships that could have appeared to influence the work reported in this paper.

Acknowledgement

The National Research Foundation of Korea Grant funded by the Korean Government (NRF-2018R1A2B2005519) supported this work.

Appendix. Statistical data of displacement and rotation with the different intensity levels

PGA(g)	Displacement						Rotation					
	max disp (m)	IA (degrees)	min disp (m)	IA (degrees)	Mean (m)	Cov(%)	max rot (m)	IA (degrees)	min rot (m)	IA (degrees)	Mean (m)	Cov(%)
Tabas												
0.1	0.741	70	0.553	170	0.665	0.097	0.621	70	0.446	160	0.552	0.104
0.3	1.249	70	0.773	170	1.094	0.171	1.117	60	0.659	160	0.951	0.166
0.5	1.797	60	1.005	170	1.553	0.216	1.591	60	0.874	160	1.322	0.197
1	3.343	70	1.737	170	2.728	0.223	2.695	70	1.397	170	2.190	0.219
Imperial Valley												
0.1	0.596	90	0.477	180	0.549	0.067	0.481	100	0.379	180	0.438	0.075
0.3	0.908	90	0.551	180	0.759	0.140	0.749	90	0.458	180	0.627	0.147
0.5	1.219	90	0.625	180	0.955	0.178	0.981	90	0.540	180	0.794	0.172
1	1.997	90	0.813	180	1.394	0.239	1.553	100	0.752	180	1.152	0.205
Loma Prieta												
0.1	0.503	170	0.467	60	0.486	0.027	0.421	160	0.374	60	0.396	0.040
0.3	0.630	170	0.523	60	0.579	0.067	0.582	160	0.445	60	0.508	0.092
0.5	0.777	170	0.579	60	0.675	0.107	0.736	160	0.517	60	0.616	0.122
1	1.288	180	0.742	60	1.003	0.216	1.105	170	0.691	50	0.902	0.173
Northridge												
0.1	0.502	90	0.461	80	0.482	0.024	0.400	110	0.360	80	0.386	0.031
0.3	0.629	90	0.501	80	0.565	0.063	0.524	70	0.402	80	0.477	0.076
0.5	0.752	90	0.543	80	0.645	0.090	0.646	70	0.444	80	0.568	0.106
1	1.179	90	0.644	80	0.868	0.173	0.977	70	0.550	80	0.797	0.157
Kobe												
0.1	0.549	150	0.459	80	0.521	0.043	0.449	0	0.360	80	0.428	0.060
0.3	0.744	150	0.496	80	0.671	0.090	0.657	0	0.401	80	0.596	0.121
0.5	0.943	150	0.534	80	0.821	0.123	0.843	0	0.443	80	0.751	0.145
1	1.700	180	0.625	80	1.251	0.197	1.390	170	0.542	80	1.121	0.177

References

Ahn, D., Shin, S.C., Kim, S.Y., Kharoufi, H., Kim, H.C., 2017. Comparative evaluation of different offshore wind turbine installation vessels for Korean west–south wind farm. Int. J. Nav. Archit. Ocean Eng. 9, 45–54. https://doi.org/10.1016/j.ijnaoe.2016.07.004.

Ancheta, T.D., Bozorgnia, Y., Chiou, B.S.-J., Stewart, J.P., Boore, D.M., Graves, R.W., Abrahamson, N.A., Campbell, K.W., Idriss, I.M., Youngs, R.R., Atkinson, G.M., 2012. PEER NGA-west 2 Database : a database of ground motions recorded in shallow crustal earthquakes in active tectonic. 15th World Conf. Earthq. Eng.

Andreotti, G., Lai, C.G., 2017. A nonlinear constitutive model for beam elements with cyclic degradation and damage assessment for advanced dynamic analyses of geotechnical problems. Part II: validation and application to a dynamic soil–structure interaction problem. Bull. Earthq. Eng. 15, 2803–2825. https://doi.org/10.1007/s10518-017-0091-0.

Asareh, M.A., Schonberg, W., Volz, J., 2016. Fragility analysis of a 5-MW NREL wind turbine considering aero-elastic and seismic interaction using finite element method. Finite Elem. Anal. Des. 120, 57–67. https://doi.org/10.1016/j.finel.2016.06.006.

Asareh, M.A., Schonberg, W., Volz, J., 2015. Effects of seismic and aerodynamic load interaction on structural dynamic response of multi-megawatt utility scale horizontal axis wind turbines. Renew. Energy 86, 49–58. https://doi.org/10.1016/j.renene.2015.07.098.

Athanatopoulou, A.M., 2005. Critical orientation of three correlated seismic components. Eng. Struct. 27, 301–312. https://doi.org/10.1016/j.engstruct.2004.10.011.

Baker, J.W., 2015. Efficient analytical fragility function fitting using dynamic structural analysis. Earthq. Spectra 31.

Cao, A.T., Tran, T.T., Nguyen, T.H.X., Kim, D., 2019. Simplified approach for seismic risk assessment of cabinet facility in nuclear power plants based on cumulative absolute velocity. Nucl. Technol. 206, 1–15. https://doi.org/10.1080/00295450.2019.1696643.

Clough, R.W., Benuska, K.L., 1967. Nonlinear earthquake behavior of tall buildings. J. Eng. Mech. Div. 93, 129–146.

Dueñas-Osorio, L., Basu, B., 2008. Unavailability of wind turbines due to wind-induced accelerations. Eng. Struct. 30, 885–893. https://doi.org/10.1016/j.engstruct.2007.05.015.

Ellingwood, B.R., Celik, O.C., Kinali, K., 2007. Fragility assessment of building structural systems in Mid-America. Earthq. Eng. Struct. Dynam. 36, 1935–1952. https://doi.org/10.1002/eqe.693.

Feyzollahzadeh, M., Mahmoodi, M.J., Yadavar-Nikravesh, S.M., Jamali, J., 2016. Wind load response of offshore wind turbine towers with fixed monopile platform. J. Wind Eng. Ind. Aerod. 158, 122–138. https://doi.org/10.1016/j.jweia.2016.09.007.

Hussan, M., Rahman, M.S., Sharmin, F., Kim, D., Do, J., 2018. Multiple tuned mass damper for multi-mode vibration reduction of offshore wind turbine under seismic excitation. Ocean. Eng. 160, 449–460. https://doi.org/10.1016/j.oceaneng.2018.04.041.

Jonkman, J., Butterfield, S., Musial, W., Scott, G., 2009. Definition of a 5-MW Reference Wind Turbine for Offshore System Development.

Jonkman, J.M., 2009. Dynamics of offshore floating wind turbines-model development and verification. Wind Energy 12, 459–492. https://doi.org/10.1002/we.347.

Kim, D.H., Lee, S.G., Lee, I.K., 2014. Seismic fragility analysis of 5MW offshore wind turbine. Renew. Energy 65, 250–256. https://doi.org/10.1016/j.renene.2013.09.023.

Kjørlaug, R.A., Kaynia, A.M., Elgamal, A., 2014. Seismic response of wind turbines due to earthquake and wind loading. Proceedings of the EURODYN 9th International Conference on Structural Dynamics. Porto, Portugal.

Kojima, K., Takewaki, I., 2016. Closed-form critical earthquake response of elastic–plastic structures on compliant ground under near-fault ground motions. Front. Built Environ 2, 1. https://doi.org/10.3389/fbuil.2016.00001.

Kojima, K., Takewaki, I., 2015. Critical earthquake response of elastic–plastic structures under near-fault ground motions (Part 1: fling-step input). Front. Built Environ. 1, 12. https://doi.org/10.3389/fbuil.2015.00012.

Lai, W.-J., Lin, C.-Y., Huang, C.-C., Lee, R.-M., 2016. Dynamic analysis of jacket substructure for offshore wind turbine generators under extreme environmental conditions. Appl. Sci. 6, 307. https://doi.org/10.3390/app6100307.

Li, H., Hu, Z., Wang, J., Meng, X., 2018. Short-term fatigue analysis for tower base of a spar-type wind turbine under stochastic wind-wave loads. Int. J. Nav. Archit. Ocean Eng. 10, 9–20. https://doi.org/10.1016/j.ijnaoe.2017.05.003.

Meng, X., Chen, G., Zhu, G., Zhu, Y., 2019. Dynamic quantitative risk assessment of accidents induced by leakage on offshore platforms using DEMATEL-BN. Int. J. Nav. Archit. Ocean Eng. 11, 22–32. https://doi.org/10.1016/j.ijnaoe.2017.12.001.

Murtagh, P.J., Basu, B., Broderick, B.M., 2005. Along-wind response of a wind turbine tower with blade coupling subjected to rotationally sampled wind loading. Eng. Struct. 27, 1209–1219. https://doi.org/10.1016/j.engstruct.2005.03.004.

Nguyen, P.C., Kim, S.E., 2018. A new improved fiber plastic hinge method accounting for lateral-torsional buckling of 3D steel frames. Thin-Walled Struct. 127, 666–675. https://doi.org/10.1016/j.tws.2017.12.031.

Nguyen, P.C., Kim, S.E., 2017. Investigating effects of various base restraints on the nonlinear inelastic static and seismic responses of steel frames. Int. J. Non Lin. Mech. 89, 151–167. https://doi.org/10.1016/j.ijnonlinmec.2016.12.011.

Nuta, E., 2010. Seismic Analysis of Steel Wind Turbine Towers in the Canadian Environment. University of Toronto, Canada.

Penzien, J., Watabe, M., 1974. Characteristics of 3-dimensional earthquake ground motions. Earthq. Eng. Struct. Dynam. 3, 365–373. https://doi.org/10.1002/eqe.4290030407.

Pham, T.D., Shin, H., 2019. Validation of a 750 kW semi-submersible floating offshore wind turbine numerical model with model test data, part I: model-I. Int. J. Nav. Archit. Ocean Eng. 11, 980–992. https://doi.org/10.1016/j.ijnaoe.2019.04.005.

Prowell, I., Elgamal, A., Jonkman, J., 2009. FAST Simulation of Wind Turbine Seismic Response.

Salman, K., Tran, T.T., Kim, D., 2020. Seismic capacity evaluation of NPP electrical cabinet facility considering grouping effects. J. Nucl. Sci. Technol. 57, 1–13. https://doi.org/10.1080/00223131.2020.1724206.

Sharmin, F., Hussan, M., Kim, D., 2017a. Effect of structural nonlinearity on probabilistic risk assessment of offshore wind turbine including inelastic soil

medium. Civ. Eng. Environ. Syst. 34, 221–237. https://doi.org/10.1080/10286608.2018.1431625.
Sharmin, F., Hussan, M., Kim, D., Cho, S.G., 2017b. Influence of soil-structure interaction on seismic responses of offshore wind turbine considering earthquake incident angle. Earthq. Struct. 13, 39–50. https://doi.org/10.12989/eas.2017.13.1.039.
Shinozuka, M., Feng, M.Q., Lee, J., Naganuma, T., 2000. Statistical analysis of fragility curves. J. Eng. Mech. 126, 1224–1231.
Smeby, W., der Kiureghian, A., 1985. Modal combination rules for multicomponent earthquake excitation. Earthq. Eng. Struct. Dynam. 13, 1–12. https://doi.org/10.1002/eqe.4290130103.
Song, H., Damiani, R., Robertson, A., Jonkman, J., 2013. New structural-dynamics module for offshore multimember substructures within the wind turbine computer-aided engineering tool FAST. Offshore and Polar Engineering Conference – ISOPE 2013. Anchorage, Alaska.
Taucer, F.F., 1991. A Fiber Beam-Column Element for Seismic Response Analysis of Reinforced Concrete Structures.
Tran, T.-T., Cao, A.-T., Kim, D.. VC4OWT: MATLAB interface for vibration control of offshore wind turbine 530-536. https://doi.org/10.1007/978-981-13-2306-5_75.
Tran, T.-T., Nguyen, T.-H., Kim, D., 2018. Seismic incidence on base-isolated nuclear power plants considering uni- and bi-directional ground motions. J. Struct. Integr. Maint. 3, 86–94. https://doi.org/10.1080/24705314.2018.1461547.
Tran, T., Nguyen, T., Park, J., Kim, D., 2017. Nonlinear behaviour of reinforced concrete structures using incremental dynamic analysis considering height effects. The 8th Asia and Pacific Young Researchers and Graduates Symposium (YRGS 2017) (Tokyo, Japan).
Vamvatsikos, D., Cornell, C.A., 2002. Incremental dynamic analysis. Earthq. Eng. Struct. Dynam. 31, 491–514. https://doi.org/10.1002/eqe.141.
Van Tu, N., Kim, D., 2013. Influence of incident angles of earthquakes on inelastic responses of asymmetric-plan structures. Struct. Eng. Mech. 45, 369–385. https://doi.org/10.12989/sem.2013.45.3.373.
Vemula, N.K., DeVries, W., Fischer, T., Cordle, A., Schmidt, B., 2010. Design Solution for the Upwind Reference Offshore Support Structure.
Wilson, E.L., Button, M.R., 1982. Three-dimensional dynamic analysis for multi-component earthquake spectra. Earthq. Eng. Struct. Dynam. 10, 471–476. https://doi.org/10.1002/eqe.4290100309.
Witcher, D., 2005. Seismic analysis of wind turbines in the time domain. Wind Energy 8, 81–91. https://doi.org/10.1002/we.135.
Zhang, J., Huo, Y., 2009. Evaluating effectiveness and optimum design of isolation devices for highway bridges using the fragility function method. Eng. Struct. 31, 1648–1660. https://doi.org/10.1016/j.engstruct.2009.02.017.
Zuo, H., Bi, K., Hao, H., 2017. Using multiple tuned mass dampers to control offshore wind turbine vibrations under multiple hazards. Eng. Struct. 141, 303–315. https://doi.org/10.1016/j.engstruct.2017.03.006.